Int. J. Electrochem. Sci., 17 **(2022)** Article Number: 221243, doi: 10.20964/2022.12.44

International Journal of
ELECTROCHEMICAL
SCIENCE
www.electrochemsci.org

Roles of *β* phase on AZ91D Magnesium Alloy Pit Corrosion: *In Situ* Study by Electrochemical Noise Analysis and Scanning Electrochemical Microscopy

Hanchun Wang[1], *Yanan Cui*[1], *Jidong Wang*[2,*], *Bin Liu*[1]

[1] Faculty of Materials Science and Chemical Engineering, Harbin Engineering University, Ministry of Education, Nantong ST 145, Harbin, 150001, China
[2] Shenyang National Laboratory for Materials Science, Northeastern University, 3-11 Wenhua Road, Shenyang, 110819, China
[*]E-mail: wangjidong@stumail.neu.edu.cn

Received: 30 September 2022 / *Accepted:* 8 November 2022 / *Published:* 30 November 2022

Electrochemical noise (EN) analysis was used to investigate the influence of the *β* phase on AZ91D alloy pit corrosion. The results revealed that the *β* phase was involved in AZ91D alloy pit corrosion in two ways: (1) during the pit initiation process, the *β* phase acted as a galvanic cathode. This *β* phase lowered the rate of nucleation but increased the transition ratio of nucleation to metastable pits. (2) After the formation of stable pits, the *β* phase was an anodic barrier that lowered the probability of pit growth, demonstrating that the pits formed on the AZ91D alloy at this point were less likely to become stable compared with T4 heat-treated AZ91D alloy. Therefore, pit cavities developed were larger than those on T4 heat-treated AZ91D alloy.

Keywords: AZ91D alloy; T4 heat-treated AZ91D alloy; Electrochemical noise; Pit corrosion; *β* phase

1. INTRODUCTION

Magnesium (Mg) is a light metal that has been get more attention for engineering applications due to its high thermal conductivity, high specific rigidity, easy recycling, and good biocompatibility [1-3]. Therefore, Mg and its alloy are highly desirable for use in aerospace and automotive applications [4, 5]. However, Mg and its alloys also have poor corrosion resistance, which is because of the high chemical reactivity of Mg and its alloy in solution or in the presence of humidity [6, 7].

Pit corrosion of Mg alloy is a major contributor to the structural failure of these alloys. Two processes lead to pit corrosion: the initiation and growth of the pits. Pit initiation is caused by random fluctuations in local environmental conditions, which leads to passive layer breakdown. When pit

nucleation happens, pits can immediately re-passivate or grow before re-passivating. This is referred to as metastable pitting. When metastable pits indefinitely grow, they become stable pits.

Mg-Al alloys are some of the most commonly used Mg alloys due to their low cost and desirable properties at 95-120 °C. A common Mg-Al alloy is AZ91D alloy [8]. Typically, the aluminum in Mg-Al alloys partially exists in solid solution and partly precipitates out of solution as a β phase ($Mg_{17}Al_{12}$). The β phase is present along the grain boundaries as a continuous phase. During the past decade, numerous studies [9-27] have reported that the β phase has a major role in AZ series alloy corrosion. Song and Atrens [9, 10] have reported that the β phase has dual roles: it acts as a galvanic cathode and enhances α matrix corrosion if the β phase is present in an excessively low volume fraction. When the β phase is present in higher volume fractions, it can inhibit overall alloy corrosion due to its anodic barrier properties. However, the roles that the β phase plays during AZ91D alloy pit corrosion are still not well-understood, and a more systematic analysis of pit corrosion is desirable. For example, what is the role of the β phase on the nucleation of pits and the transition of these pits to metastable pits? When metastable pits are formed, how does the β phase affect their growth and whether or not they become stable? The answers to these questions are still not clear.

Electrochemical noise (EN) analysis can be used to obtain fundamental knowledge about the nature of corrosion processes. Therefore, this electrochemical technique is an increasingly popular method for investigating Mg alloy corrosion processes [28-32]. A major benefit of this technology is its noninvasive nature- EN avoids artificial system disturbance. Moreover, EN analysis can be used to monitor corrosion rates and determine corrosion mechanisms [28-32]. EN also has some advantages compared to other electrochemical analysis methods: for example, EN can be used to monitor corrosion process rates in real-time [28-30]. EN can also be used to evaluate localized corrosion [30-32]. Therefore, EN is an extremely powerful method for investigating the mechanisms of pit corrosion.

The roles of the β phase on AZ91D alloy pit corrosion were investigated in this work. The pit corrosion of AZ91D alloy was evaluated by EN and compared to the pit corrosion of a corresponding T4 heat-treated AZ91D alloy.

2. EXPERIMENTAL SECTION

2.1 Materials

The alloy was AZ91D alloy in this research. The main elemental components of AZ91D alloy were: 8.5-9.5 % Al, 0.45-0.9 % Zn, 0.17-0.5 % Mn, < 0.05 % Si, < 0.004 % Fe, < 0.001 % Ni, < 0.015 % Cu, and < 5 to 15 ppm Be. A T4 heat treatment process (homogenized heat treatment) was performed on the AZ91D alloy for 16 h at 410 °C, followed by immediate quenching in water. The AZ91D alloy after T4 heat treatment is called to as the T4 heat-treated AZ91D alloy. Before each experiment, the working surface of sample was wet ground to a 2000-grit finish. Then, acetone was used to degrease the polished alloys, and distilled water was used to rinse them after degreasing. The alloys were dried under a flow of compressed heated air.

Most of the experiments were performed in 0.05 M NaCl. However, 0.05 M Na_2SO_4 was used to verify the current threshold values for the experiments. The pH value of solution used was 12.

2.2 Microstructural analysis

Micrographs of the AZ91D and T4 heat-treated AZ91D alloys were obtained by a Philips-XL30 scanning electron microscope (SEM).

2.3 Electrochemical measurement

An Autolab electrochemical workstation was used to conduct EN analysis in a Faraday cage. The workstation was equipped with an EN module. The working electrode was two identical specimens, and the reference electrode was a Ag/AgCl/KCl (saturated) electrode. When the galvanic coupling current between the two identical working electrodes (WE) was kept at the same potential, the electrochemical current noise was carried out. EN analysis was performed and data were collected for a period of 14 h. Each EN dataset contained 8192 data points, and the data sampling interval was 0.08 s. Each Mg alloy was analyzed with 168 time records.

3. RESULTS

3.1 Microstructure

The AZ91D and T4 heat-treated AZ91D alloys microstructures are displayed in Fig. 1. Aluminum was present in the solid solution with the α phase as well as in the β phase in AZ91D alloy. This β phase was mainly precipitated along the α phase grain boundaries (Fig. 1a). After T4 treatment, the β phase dissolved in the α phase (Fig. 1b).

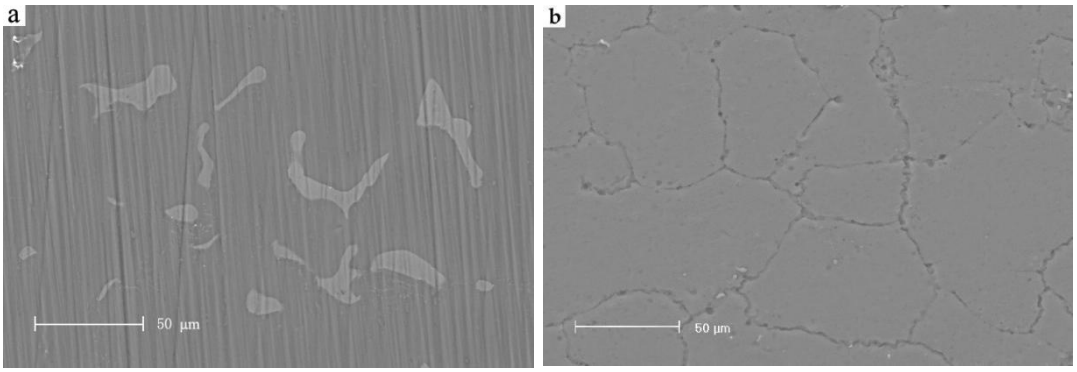

Figure 1. SEM micrographs of the (a) AZ91D and (b) T4 heat-treated AZ91D alloys.

3.2 EN records

3.2.1 Transient of pit events

The typical current noise fluctuations of the AZ91D and T4 heat-treated AZ91D alloys within an interval of 324.68 s are shown in Fig. 2. Many anodic current spikes were clearly distinguished from the

background current fluctuation. The current spikes represented nucleation or metastable pitting events. The current transients obtained from the AZ91D and T4 heat-treated AZ91D alloys were very similar.

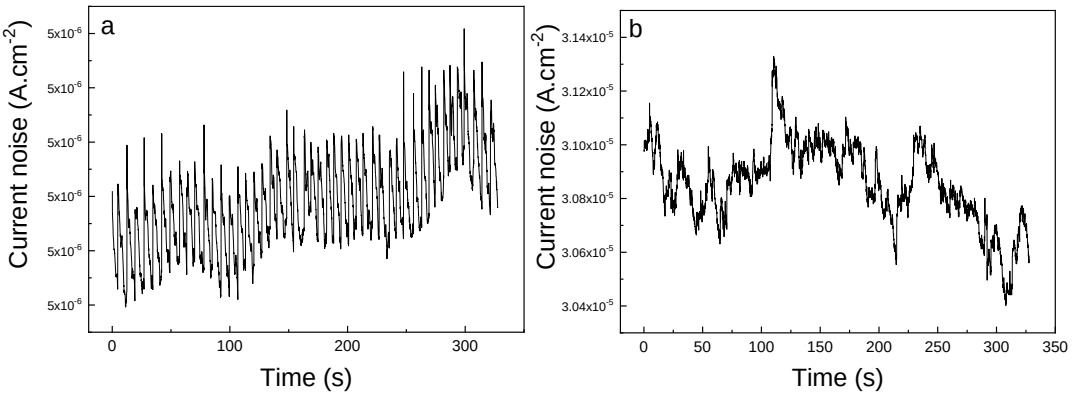

Figure 2. Typical current noise fluctuations of the (a) AZ91D and (b) T4 heat-treated AZ91D alloys in 0.05 M NaCl solution within an interval of 324.68 s.

A nucleation event was indicated by a rapid increase in current from the background level followed by a relatively gentle (but still rapid) fall to the background current noise level, as shown in Fig. 3. Nucleation, which happens extremely quickly, occurs due to the rupture of an alloy oxide film, followed by re-passivation [33, 34].

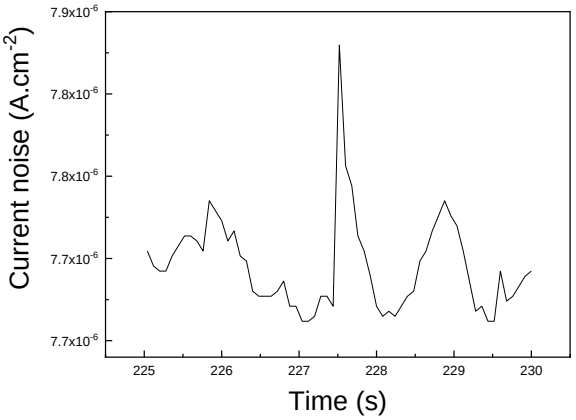

Figure 3. Current transient of Mg alloy in the nucleation process.

Figs. 4 and 5 show the two types of identified metastable pit events. The current transient caused by metastable propagation (type 1) is shown in Fig. 4. A sharp initial surge in current was observed. Next, partial current decay occurred due to the attempted re-passivation of the nucleated pit. This was the pit nucleation event. However, re-passivation was not complete, leading to a noticeably more sluggish increase in current. This gentler increase in current represented metastable pit propagation:

during this period, the pit grew via high-rate anodic dissolution. This slow increase in current over time can only be attributed to propagation. Finally, after a short propagation period, the current rapidly decayed and the pit re-passivated. The current transient caused by metastable propagation (type 2) is shown in Fig. 5. Fig. 5 displays an anodic current transient with a rapid initial rise in value, followed by a short plateau in the current prior to re-passivation. Pit initiation caused this event. Next, a very short propagation period occurred across the current plateau before the event ended due to re-passivation. The constant current of the plateau demonstrated that the metal dissolved during this period. This was because the evolved anodic charge either formed a passivating oxide (causing current decay) or led to the dissolving of ions—no other process explains this current plateau.

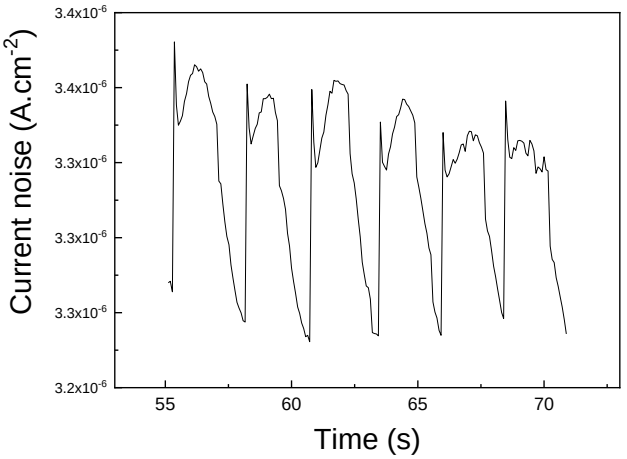

Figure 4. Current transient of magnesium alloy caused by the propagation of a single metastable pit on magnesium alloy.

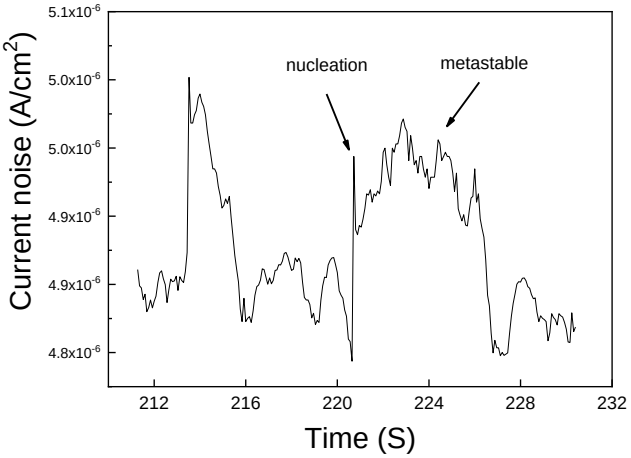

Figure 5. Anodic current transient of magnesium alloy.

3.2.2 Determination of background noise

The method reported by G.T. Burstein was used to analyze the nucleation and metastable pit transients. In this method, the number of current spikes was counted as a function of spike amplitude

and time [33-42]. Moreover, the lower limit of threshold was the digital point-to-point instrumental resolution. When the threshold was increased, the number of spikes in current above that threshold rapidly decayed toward zero in the chloride-free electrolyte. A few current spikes with a low intensity were occasionally recorded in the chloride-free electrolyte. This was attributed to equipment interference or other laboratory activities. However, because the origin of these events was clear and they were very low in number, they were ignored.

Using the chloride-containing electrolyte, the number of current spikes counted as a function of the threshold was initially the same as that obtained in the chloride-free electrolyte, as shown in Fig. 6. However, the decay became significantly more gradual as the threshold current increased. The low threshold counts also included background noise and was similar to the result in chloride-free electrolyte. The significant deviation between the two graphs indicated the position of the true threshold between the anodic current spikes and the background noise. In this work, the threshold between the background and anodic spikes was conservatively set to 5.5 nA; visual inspection of the data trains was performed to double-check this threshold. This analysis method rejected nucleation events with amplitudes below 5.5 nA because these events were not unambiguously able to be distinguished from the background noise.

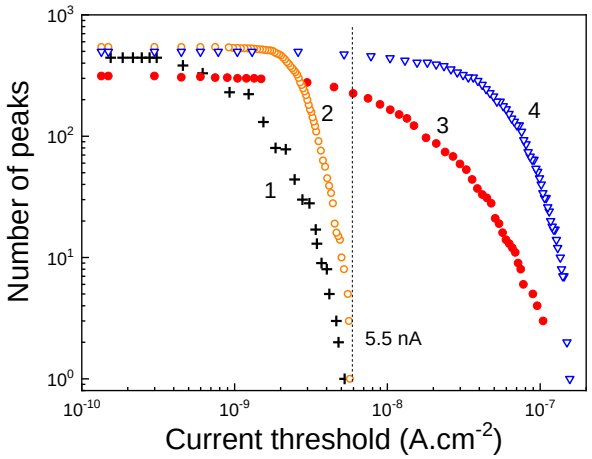

Figure 6. The threshold current of magnesium alloy immersed in the different solutions: (1) AZ91D alloy and (2) T4 heat-treated AZ91D alloys in 0.05 M Na_2SO_4; (3) AZ91D and (4) T4 heat-treated AZ91D alloys in 0.05 M NaCl.

Using this strategy to count the current spikes, the rising current transients that were more significantly sustained compared to simple nucleation spikes were identified to separately count the number of metastable pitting events. This was different from the counting method used for nucleation spikes, which simply involved determining that the difference between adjacent data points was greater than a set threshold. The nucleation spike count reported in this work includes the spikes that became metastable pits. The current spikes that terminated metastable growing pits (Figs. 4 and 5) were removed. However, the exclusion or inclusion of these spikes in the counting process did not significantly affect

these results because the number of total nucleation events was significantly higher than the number of metastable growing pits.

4. DISCUSSION

Generally, the rate of pit initiation (nucleation and metastable pits) and the probability of pit growth influence the susceptibility of an alloy to pitting corrosion. This probability determines how pits form and whether or not they become stable. If an alloy displays a higher rate of pit initiation, metastable pits will grow and spread across the alloy surface. If an alloy has a higher probability of pit growth, the pits formed on this alloy more easily turn into large cavities. Stable pits are formed when the metastable pit volumes exceed a certain value. The size and number of precipitates have an important influence on the metastable pits [43, 44].

4.1 Roles of β phase on nucleation and the transition to metastable pits

The average nucleation frequency of the AZ91D and T4 heat-treated AZ91D alloys is shown in Fig. 7. The 14 hours of the experiment represented 1.376×10^6 data points, and this data were divided into 14 segments that each contained 98304 data points. Each segment represented a period of 1 h. The pit formation process was assumed to follow a Poisson relationship, in which the numbers of events that occurred during the 14 non-overlapping segments were random independent variables [45,46]. Data point regression was used with Eqs. (1) and (2) to calculate and summarize the initial frequency of events (λ_0), the time constant (τ), and the total number of available events (N_0), as shown in Table 1:

$$\lambda = \lambda_0 \exp(-\frac{t}{\tau}) \quad (1)$$

$$N_0 = \lambda_0 \tau \quad (2)$$

where λ is the nucleation rate.

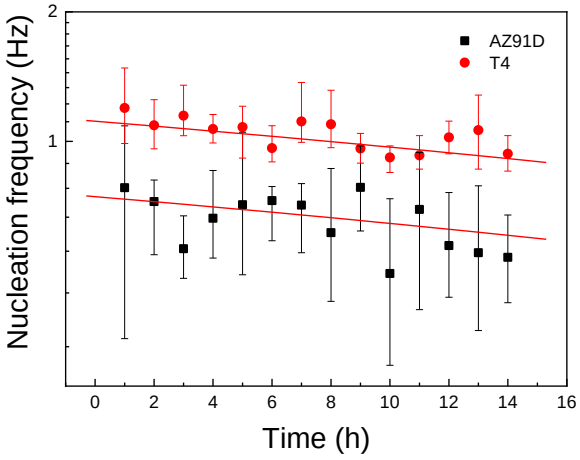

Figure 7. Average nucleation event frequency vs. time for the AZ91D and T4 heat-treated AZ91D alloys.

The λ_0 and N_0 values of the AZ91D alloy were lower than those of the T4 heat-treated AZ91D alloy (Table 1). Therefore, the AZ91D alloy was less susceptible to pit nucleation than the T4 heat-treated AZ91D alloy. The AZ91D alloy had a higher τ value than the T4 heat-treated AZ91D alloy, meaning that nucleation proceeded for a longer time on the AZ91D alloy. This demonstrated that the imitation of nucleation on the AZ91D alloy was more difficult and the AZ91D alloy exhibited a significant ability to resist pit nucleation. These results revealed that the presence of the β phase inhibited the nucleation rate.

Table 1. The parameters obtained by data point regression.

	AZ91D alloy	T4 heat-treated AZ91D alloy
λ ($s^{-1}cm^{-2}$)	0.750	1.153
τ(s)	1.791×10^5	2.582×10^5
N_0	1.344×10^5	2.978×10^5

The average metastable pit event frequencies in NaCl solution on the AZ91D and T4 heat-treated AZ91D alloys are shown in Fig. 8. The T4 heat-treated AZ91D alloy was the more active in terms of metastable pit formation, which was consistent with its pit nucleation behavior.

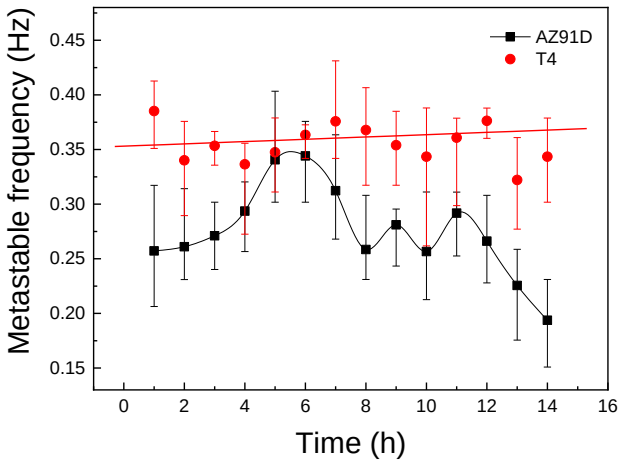

Figure 8. Average metastable event frequencies for the AZ91D and T4 heat-treated AZ91D alloys as a function of time.

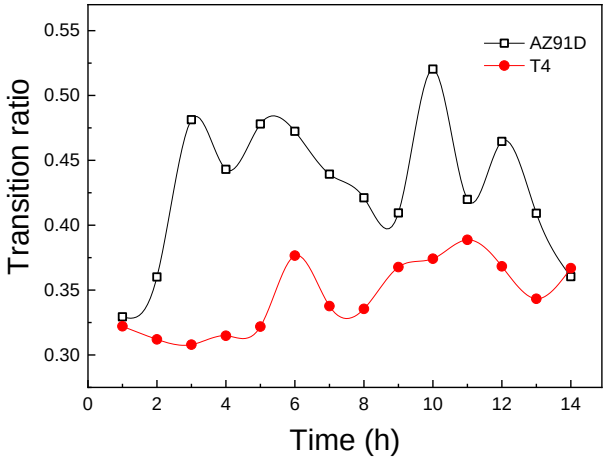

Figure 9. Transition ratio of nucleation to metastable pits for the AZ91D and T4 heat-treated AZ91D alloys as a function of time.

However, the transition ratio of nucleation to metastable pits should also be taken into consideration. The transition ratio was lower for the T4 heat-treated AZ91D alloy, indicating that the propagation of metastable pits was much more difficult on T4 heat-treated AZ91D alloy. This implied that the existence of the β phase led to a higher metastable pit propagation probability (Fig. 9).

Pit nucleation is related to the impurity sites of alloys. Ralson et al. found the metastable pits are related to the number of precipitates [47]. Therefore, the total number of nucleations (N_0) was related to the number of alloy surface impurities. However, the number of nucleations is only equal to the number of impurities available on the surface of alloy if there is a one-to-one ratio between the two-i.e., one impurity is removed by a single nucleation event. This might be possible for some impurities, especially if they are small. However, it is not likely that all impurities are removed in this manner. Instead, multiple nucleation might be generated on each individual impurity before the impurity site in question is removed (assuming no metastable pit formation). Therefore, it was assumed that the number of nucleation occurring on the surfaces of the alloys was higher than the real number of alloy surface impurity sites.

It is well known that the free corrosion potentials of α phase and β phase are about -1.6 V and -1.3 V in NaCl solution, respectively. The corrosion potential difference of α phase and β phase is 0.3 V [20, 21]. The α phase corrosion occurs because it has a more highly negative free corrosion potential. Thus, the corrosion rate of α phase can be enhanced by micro-galvanic coupling between α phase and β phase.

After T4 heat treatment, the β phase was dissolved into the α phase, indicating the removal of the micro-galvanic effect. The similar results were also proved by Zhang et al [48]. Therefore, it was believed that the number of nucleation on the surface of the T4 heat-treated AZ91D alloy was higher than the real number of impurity sites. This led to a higher nucleation frequency on the surface of T4 heat-treated AZ91D alloy. However, due to the micro-galvanic coupling effect between the α and β phases in the AZ91D alloy, the anodic dissolution rate of nucleation at impurity sites was significantly accelerated, which indicated that the re-passivation of nucleation was inhibited and that metastable pit

formation was propagated. Moreover, this also manifested that most of the impurities were exhausted by one nucleation instead of several nucleation. This explains why a lower nucleation frequency and higher nucleation to metastable pit transition ratio were observed in the AZ91D alloy compared with the T4 heat-treated AZ91D alloy. Zhang et al. also [48] found the heat-treated Mg alloy has lower nucleation rate.

4.2 Pit growth probability: roles of the β phase

The current transient versus time curves were integrated to obtain the amount of charge attributed to every current transient spike. These charges were caused by pit formation. Faraday's equation (Eq. 3) was used to relate the charges to the physical pit volumes. This equation correlated the anodic current transient charge to the physical pit size [49]. It was assumed that the pits were hemispherically shaped, so the pit depth/radius were obtained with Eq. 4.

$$V(cm^3) = \frac{q \times M}{F \times n \times \rho} \qquad (3)$$

$$d_{pit}(\mu m) = \left(\sqrt[3]{\frac{3V(cm^3)}{2\pi}}\right) \times 2 \times 10000 \qquad (4)$$

where V is the pit cavity volume, q is the charge associated with a current transient, M is the molecular mass, F is the Faraday constant, ρ is the density, and d_{pit} is the pit cavity diameter. The largest pit size observed in every EN segment was calculated, and these values were statistically analyzed in more detail.

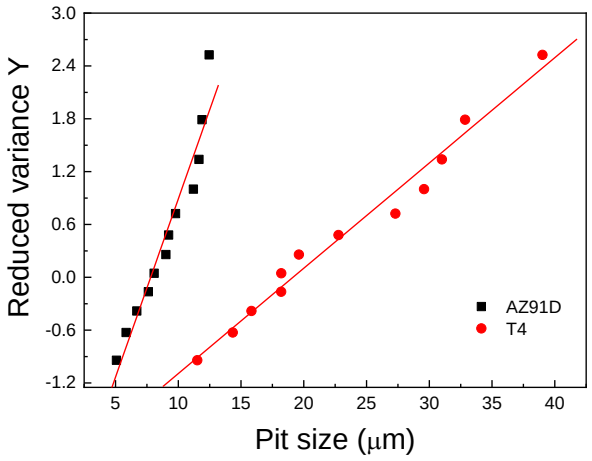

Figure 10. Typical Gumbel probability plots for the AZ91D and T4 heat-treated AZ91D alloys.

The growth of pits was modeled with a nonhomogeneous Markov process [50]. Recently, the Gumbel extreme value distribution has been used for modeling pit growth processes [51]. The Gumbel distribution of pit growth was used to describe the relationship between the reduced variant (Y) and the pit size (d_{pit}). The Y values were calculated with Eq. (5):

$$Y = -\ln[-\ln(1 - \frac{i}{N+1})] = \frac{1}{\alpha} d_{pit} - \frac{\mu}{\alpha} \qquad (5)$$

where N is the total number of extreme value data, i is the ordered extreme value rank (i=1,2,3…N), μ is the central parameter (the most frequent value), d_{pit} is the pit size, and α is the scale parameter (defining the distribution width).

Table 2. The values of α and μ for the AZ91D alloy and T4 heat-treated AZ91D alloy.

AZ91D alloy		T4 heat-treated AZ91D alloy	
α	μ	α	μ
6.405	5.491	4.693	5.621
4.294	11.294	4.027	7.563
8.363	19.144	2.473	7.802
5.581	15.355	1.683	4.787
5.516	18.097	0.947	3.666
3.875	14.456	7.293	10.062
2.523	13.845	2.125	12.768
6.027	14.504	0.874	13.383
8.939	16.646	1.165	12.244
2.187	18.501	3.201	8.171
4.573	16.892	4.789	6.758
6.208	7.935	1.270	10.211
4.663	10.652	6.092	12.229
3.870	7.176	0.300	5.779

A double exponent (Gumbel Type extreme value distribution) was used to determine the probability that the greatest pit depth was greater than x. This was determined by Eq. (6) [51].

$$P = 1 - \exp\{-\exp[\frac{-(d_{pit}-[\mu+\alpha \ln S])}{\alpha}]\} \quad (6)$$

where P is the pit size probability and d_{pit} is the pit cavity diameter.

14 segments were obtained by dividing the experimental data points into 1 h segments. In each segment, a Y value versus maximum pit size curve was plotted. A typical plot is shown in Fig. 10. The observed straight lines proved that this data was indeed described by the Gumbel distribution. The α and μ values for each segment were obtained and are shown in Table 2.

Eq. (6) was used to determine the probabilities of a specific pit size occurring on both the AZ91D and T4 heat-treated AZ91D alloys during various immersion periods. These probabilities are plotted in Fig. 11. The pit growth probability on the T4 heat-treated AZ91D alloy during the immersion period was higher, which demonstrated that the metastable pits formed on the T4 heat-treated AZ91D alloy were more likely to become stable. These stable pits would then develop into larger pit cavities across a shorter time interval compared to those on the AZ91D alloy. This is similar to the conclusion that the depth and size of the pit increased on the T6 heat-treated AlSi10Mg alloy by Wei et al[52]. This also indicated the β phase significantly influenced pit growth on the Mg alloy. The network β phase was potentially an anodic barrier, inhibiting pit growth [9]. This could explain the lower pit growth probability of the AZ91D alloy compared to the T4 heat-treated AZ91D alloy. The similar results were also proved by Zhang et al [53].

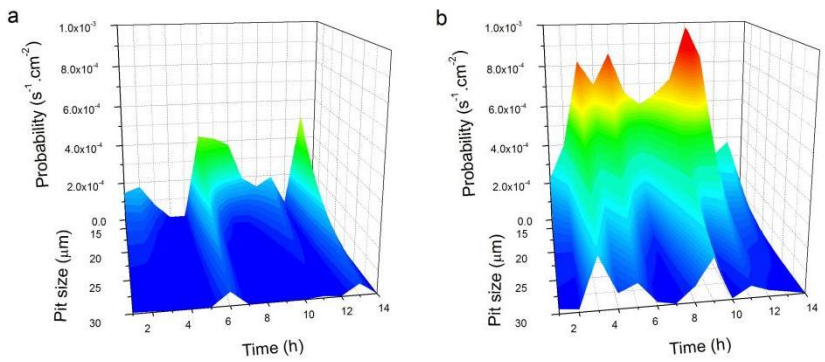

Figure 11. Probability of the formation of stable pits with various diameters on the (a) AZ91D and (b) T4 heat-treated AZ91D alloys.

5. CONCLUSION

The presence of the β phase influenced AZ91D alloy pit corrosion in two ways. One, the β phase played a galvanic cathode role during pit initiation. The existence of the β phase during this process lowered the nucleation rate but increased the transition ratio of nucleation to metastable pits. Once stable pits were formed, the β phase was able to act as an anodic barrier, lowering the probability of pit growth. This indicated that it was more difficult for the pits formed on the AZ91D alloy to become stable. Therefore, these pits were less likely to develop into large pit cavities across a shorter time interval compared with the pits on the T4 heat-treated AZ91D alloy.

ACKNOWLEDGEMENT
The authors wish to acknowledge the financial support of the National Natural Science Foundation of China (No. 50601007), the financial support of the Key Laboratory of Superlight Material and Surface Technology (Harbin Engineering University), Ministry of Education.

References

1. Z.Z. Yin, Z.Q. Zhang, X.J. Tian, Z.L. Wang, and R.C. Zeng, *Acta Metallurgica Sinica (English Letters)*, 34 (2021) 25-38.
2. R. Chalisgaonkar, Mater. *Today Proc.* 26 (2020) 1060.
3. J.H. Wang, L. Xu, R.Z. Wu, J. Feng, J.H. Zhang, L.G. Hou, and M.L. Zhang, *Acta Metall. Sin. - Engl. Lett.*, 33 (2020) 490.
4. G.R. Argade, S. Sanders, G. Mohandass, A. Alsaleh, F.D. Souza, T.D. Golden, and R.S. Mishra, *J. Mater. Eng. Perform.*, 28 (2019) 852-862.
5. Y. Li, X.P. Lu, K.X. Wu, L. Yang, T. Zhang, and F.H. Wang, *Corros. Sci.*, 168 (2020) 108559.
6. M. Esmaily, J.E. Svensson, S. Fajardo, N. Birbilis, G.S. Frankel, S. Virtanen, R. Arrabal, S. Thomas, and L.G. Johansson, *Prog. Mater. Sci.*, 89 (2017) 92–193.
7. C.Y. Zhang, S.J. Liao, B.X. Yu, X.P. Li, X.B. Chen, T. Zhang, and F.H. Wang, *Corros. Sci.*, 150 (2019) 279–295.
8. B. Mordike, and T. Ebert, *Mater. Sci. Eng. A*, 302 (2001) 37-45.

9. G. Song, A. Atrens, and M. Dargusch, *Corros. Sci.*, 41 (1999) 249-273.
10. G. Song, A. Atrens, X. Wu, and B. Zhang, *Corros. Sci.*, 40 (1998) 1769-1791.
11. M. Zhao, M. Liu, G. Song, and A. Atrens, *Corros. Sci.*, 50 (2008) 1939-1953.
12. Z. Shi, G. Song, and A. Atrens, *Corros. Sci.*, 47 (2005) 2760-2777.
13. G. Song, *Adv. Eng. Mater.*, 7 (2005) 563-586.
14. G. Song, and A. Atrens, *Adv. Eng. Mater.*, 5 (2003) 837-858.
15. G. Song, A. Bowles, and D. StJohn, *Mater. Sci. Eng. A*, 366 (2004) 74-86.
16. S. Mathieu, C. Rapin, J. Steimetz, and P. Steimetz, *Corros. Sci.*, 45 (2003) 2741-2755.
17. S. Mathieu, C. Rapin, J. Hazan, and P. Steinmetz, *Corros. Sci.*, 44 (2002) 2737-2756.
18. A. Pardo, M.C. Merino, A.E. Coy, R. Arrabal, F. Viejo, and E. Matykina, *Corros. Sci.*, 50 (2008) 823-834.
19. A. Pardo, M.C. Merino, A.E. Coy, F. Viejo, R. Arrabal, and S. Feliú, *Electrochim. Acta*, 53 (2008) 7890-7902.
20. R. Ambat, N. Aung, and W. Zhou, *Corros. Sci.*, 42 (2000) 1433-1455.
21. O. Lunder, J. Lein, T. Aune, and K. Nisancioglu, *Corrosion*, 45 (1989) 741-748.
22. T. Zhang, Y. Li, and F. Wang, *Corros. Sci.*, 48 (2006) 1249-1264.
23. M. Anik, and G. Celikten, *Corros. Sci.*, 49 (2007) 1878-1894.
24. M. Jönsson, D. Thierry, and N. LeBozec, *Corros. Sci.*, 48 (2006) 1193-1208.
25. G. Ballerini, U. Bardi, R. Bignucolo, and G. Ceraolo, *Corros. Sci.*, 47 (2005) 2173-2184.
26. R. Singh Raman, N. Birbilis, and J. Efthimiadis, *Corros. Eng. Sci. Tech.*, 39 (2004) 346-350.
27. G. Baril, C. Blanc, and N. Pébère, *J. Electrochem. Soc.*, 148 (2001) B489-B496.
28. T. Zhang, C. Chen, Y. Shao, G. Meng, and F. Wang, *Electrochim. Acta*, 53 (2008) 7921-7931.
29. T. Zhang, Y. Shao, G. Meng, and F. Wang, *Electrochim. Acta*, 53 (2007) 561-568.
30. A.M. Lafront, W. Zhang, S. Jin, R. Tremblay, D. Dubé, and E. Ghali, *Electrochim. Acta*, 51 (2005) 489-501.
31. W. Zhang, S. Jin, E. Ghali, R. Tremblay, M. Shehata, and E. Es-Sadiqi, *Adv. Eng. Mater.*, 8 (2006) 973-980.
32. S. Amira, A. Lafront, D. Dubé, R. Tremblay, and E. Ghali, *Adv. Eng. Mater.*, 9 (2007) 973-980.
33. G. Ilevbare, and G. Burstein, *Corros. Sci.*, 43 (2001) 485-513.
34. G. Ilevbare, and G. Burstein, *Corros. Sci.*, 45 (2003) 1545-1569.
35. G. Burstein, *ECS Transactions*, 3 (2006) 193-204.
36. G. Burstein, and C Liu, *Corros. Sci.*, 50 (2008) 2-7.
37. A. Moshaweh, and G. Burstein, *Corros. Sci.*, 113 (2016) 126-132.
38. G. Burstein, H. Bi, and G.Kawaley, *Electrochim. Acta*, 191 (2016) 247-255.
39. H. Bi, G. Burstein, B.B.Rodrigueza, and G.Kawaley, *Corros. Sci.*, 102 (2016) 510-516.
40. G. Burstein, and R. Souto, *J. Electrochem. Soc.*, 151 (2004) B537-B542.
41. G. Burstein, and S. Vines, *J. Electrochem. Soc.*, 148 (2001) B504-B516.
42. G. Burstein, C. Liu, R. Souto, and S. Vines, *Corros. Eng. Sci. Tech.*, 39 (2004) 25-30.
43. L. Guan, Y. Zhou, B. Zhang, J. Q. Wang, E. Han, W. Ke, Corros. Sci., 103 (2016) 255-267.
44. R. Gupta, A. Deschamps, M. Cavanaugh, S. P. Lynch, N. Birbilis, *Electrochim. Soc.*, 159 (2021) C 492-C502.
45. A. Valor, F. Caleyo, L. Alfonso, D. Rivas, and J. Hallen, Corros. Sci., 49 (2007) 559-579.
46. T. Zhang, X.L. Liu, Y.W. Shao, G.Z. Meng, and F.H. Wang, Corros. Sci., 50 (2008) 3500-3507.
47. K. D. Ralston, N. Birbilis, M. K. Cavanaugh, M. Weyland, B. C. Muddle, R Marceau, *Electrochim. Acta*, 55 (2010) 7834-7842.
48. Z. Zhang, L. Wang, R. Zhang, D. Yin, Z. Zhao, P. Bai, B. Liu, and F. Wang, *J. Mater. Res. Technol.*, 18 (2022) 416-427.
49. S. Pride, J. Scully, and J. Hudson, *J. Electrochem. Soc.*, 141 (1994) 3028-3040.
50. A. Valor, F. Caleyo, L. Alfonso, D. Rivas, and J. Hallen, *Corros. Sci.*, 49 (2007) 559-579.
51. E.J. Gumbel, *Statistics of Extremes*, Columbia University Press, NY, (1957).

52. P. Wei, Z. Chen, S.Z. Zhang, X.W. Fang, B.H. Lu, L.J. Zhang, and Z.Y. Wei, Mater. Charact., 171 (2021) 110769.
53. H. Zhang, D.D. Gu, D.H. Dai, C.L. Ma, Y.X. Li, M.Z. Cao, and S.H. Li, Appl. Surf. Sci., 509 (2020) 145330.